EURASIAN JOURNAL OF MATHEMATICAL AND COMPUTER APPLICATIONS
ISSN 2306–6172
Volume 12, Issue 3 (2024) 91 – 104

TURBULENT IMPINGING AIR JET FOR COOLING THE HEATED SURFACE

Mungalov A. S., Sibiryakov N. E., Kochkin D. Y., Cheverda V.V., Somwanshi P. M., Kabov O. A.

Abstract The present work deals with the experimental and numerical study of steady-state conjugate heat transfer during impingement of turbulent air jet over a heated stainless steel. The plate is heated using copper heater located at the middle. The temperature field is measured using an infrared camera and compared with the numerical simulations. Numerical simulations are performed using three-dimensional finite volume based formulation. The turbulence shear-stress transport (SST) is modeled using $k-\omega$ model based on the Reynolds averaged Navier Stokes (RANS) equations. The numerical simulations are in good agreement with the experimental data with marginal discrepancy in the steel plate region due to the contact thermal resistance between steel and copper. It is observed that the local Nusselt number increased in the stagnation region with increasing velocity of the impinging turbulent flow and practically unaltered in the region of the steel plate.

Key words: impinging jet, turbulence modeling, heat transfer, numerical simulations, RANS.

AMS Mathematics Subject Classification: 76D25.

DOI: 10.32523/2306-6172-2024-12-3-91-104

1 Introduction

A directed stream of liquid or gas ejected onto or along a surface can effectively transfer large amounts of heat between the surface and the fluid. Promising cooling methods that involve one or multiple phases directly in contact with the heating element include mini and microchannel [1-4] systems, gas and liquid jets, spray [5]. Heat transfer include annealing of metals, cooling of electronic components, tempering of glass, preventing of fogging, cooling of turbines and engines, drying of materials and other processes [6]. In applications, where direct liquid cooling is not possible or inconvenient, an impact air jet can be used. The parameters of impacting jets and their applications in heat transfer have long been discussed in research and review articles [7].

The jet upon exiting the nozzle is divided into several stage such as exiting from the nozzle and the formation of a turbulent jet during interaction with the surrounding air, movement of the formed jet, falling onto a solid surface with the movement near the stagnation point, spreading over a solid surface [8]. Moreover, the flow structure and local heat transfer depend on many parameters such as the Reynolds number, the distance from the nozzle to the surface, the shape of the nozzle and the geometry of the heater [9]. For small heater sizes, one of the determining heat transfer processes is heat transfer in the boundary layer near the stagnation point. The movement of fluid in the boundary layer near the symmetry axis can be approximately described by the equations:

$$v_z = -\alpha z^2 \tag{1}$$

$$v_r = \alpha z r \tag{2}$$

where α is an empirical constant, z is vertical coordinate and r is radial coordinate. Zero of the coordinate system is at the center of impact on the solid surface.

The full velocity profiles are much more complex [10], but the asymptotic representation shows that heat transfer from the surface is significantly complicated by the sharp decrease in the radial and vertical velocity components.

Although empirical and semi-empirical models exist to describe the flow and heat transfer of impacting jets [8, 11, 12], they do not accurately predict the heat transfer efficiency for a particular cooling device configuration, especially if the heater has an complex/unusual geometry. Therefore, it is necessary to improve numerical methods for calculating the interaction of turbulent jets with a substrate.

The literature features numerous experimental works and numerical simulations approaches focusing on various configurations of cooling utilizing turbulent impinging jets. Widely used semi-empirical correlations as well as their relative advantages and drawbacks of the $k-\epsilon$, $k-\omega$, Reynolds stress model, algebraic stress models, shear stress transport, and $v^2 - f$ turbulence models for impinging jet flow and heat transfer are compared in the review [13]. Dairay et al cerried out direct numerical simulation (DNS) of an impinging turbulent jet flow [14] with high spatial resolution employing high-order numerical techniques. They focused on spatial distribution of the heat transfer coefficient at the wall. The velocity and temperature statistics were verified against experimental data.

The influence of flow and geometrical parameters on the heat transfer during impinging jets is presented in [15-18]. The work [19] is devoted to experimental and numerical study on the heat transfer characteristics of various geometrical arrangement of impinging jet arrays. The influence of geometrical and flow parameters such as variations in jet-to-jet spacing, slot jet widths, jet-to-plate distance, and Reynolds number on the local Nusselt distribution is considered.

For a specific configuration of slot jet arrays, the local heat transfer coefficient demonstrates an increase with rising Reynolds numbers and diminishing jet-to-plate spacing. The authors of [20] proposed array of cone heat sinks and considered heat transfer enhancement during jet impingement using a single cone heat sink.

The authors concluded that the cooling efficiency of a fluid impinging on a cone-shaped heat sink surpasses that of a traditional flat plate heat sink. The influence of a pin on the flow and heat transfer characteristics resulting from a pulsating jet impinging on a heated flat surface is examined in [21]. The computational findings demonstrated that the RNG $k-\epsilon$ model is capable of accurately predicting the distribution of Nusselt numbers in accordance with experimental observations. The results showed that the Nusselt number increases with increasing pulse frequency and Reynolds number and decreases with increasing distance from the jet to the target surface. The influence of surface variations along the plates on heat transfer between impinging jets and non-uniform heated plates is considered in [22]. Using numerical simulation results, the authors offer some recommendations in improving the design of impinging jets based cooling devices. A numerical study using the shear-stress transport (SST) $k-w$ model to verify the effect of nozzle geometry and location on the impinging jets heat transfer is discussed in [23]. An elliptic relaxation turbulence model is used in [24] to simulate the heat transfer in circular confined and unconfined impinging jet configurations. Confinement results in a reduction in the overall heat transfer rates, while the local stagnation heat transfer coefficient remains constant. The study [25] deals with experimental and computational results of heat transfer coefficients in the case of impinging a synthetic jet flow. The numerical simulation of heat transfer from a flat heated surface using the impingement of a turbulent annular fluid jet is considered in [26]. It was observed that the local heat-transfer rate increases near the the impingement zone with increase in the the Reynolds number. Numerical simulation of transient coupled heat transfer in a highly turbulent air jet impinging on a flat circular disk is presented in [27]. The results indicate that the Reynolds number of the jet has a significant effect on the hydrodynamics and heat transfer, especially in the stagnant region.

The pulsation of the jet flow is known to be the effective methods to increase the heat transfer efficiency [28-30]. The numerical study conducted in [31] focuses on heat transfer phenomena within a pulsating impinging jet. The study examines the impact of various parameters, including frequency, amplitude, and geometric factors, on the heat transfer rate. Results show that flow pulsation induces varying effects within distinct flow regions. Specifically, the pulsation of the jet enhances cooling efficiency in the vicinity of the wall, while concurrently diminishing heat transfer in the stagnation region. The authors concluded that the cooling effectiveness of the oscillating jet is positively correlated with higher frequencies and amplitudes of oscillations, as well as with reduced nozzle-to-plate distances. The article [32] deals with the experimental and numerical study of local heat transfer during impingement of a synthetic jet over a flat plate. Various Reynolds numbers and pulse frequencies are considered. The peak value of the time-averaged Nusselt number is found at the stagnation point of the synthetic impinging jet for all analyzed distances from the obstacle surface. In [33] the influence of the forcing frequency on the heat transfer process of a synthetic jet is analyzed.

This paper considers the problem of cooling a locally heated region using a turbulent impact air jet. An experimental study is conducted as well as numerical simulations are performed using three-dimensional finite volume based formulation. The turbulence shear-stress transport (SST) is modeled using $k-\omega$ model based on the Reynolds averaged Navier Stokes (RANS) equations.

2 Experimental setup

The experimental setup is made to experimentally measure the heat flow and temperature of the cooled surface as shown in in Fig. 1. Air is supplied from the compressor

(Fig. 1(4)) through a flow regulator (flowmeter) (Fig. 1(5)) with known pressure (Fig. 1(6)) and has a room temperature of $T_{in} = 20°C$. Gas flows into the nozzle (Fig. 1(7)) resulting into the formation of air jet and subsequently falls onto a stainless steel plate. At the the middle of stainless steel plate. the thin end of a copper heater (Fig. 1(1)) with an area of $1cm^2$ is inserted. Heat flux is provided by 6 electric cartridge heaters (Fig. 1(2)) in the bottom end of the copper heater. The copper surface was fully covered by insulating material except top nozzle part, where heat is removed. There are thermocouples in the narrow part of the heater and in the steel plate (Fig. 1(3)) to control the surface temperature and heat flow entering the heater surface and spreading over the surface of the steel plate. From these thermocouples, the heat flux removed by the air jet and the heater surface temperature are calculated. This allows us to validate numerical simulation in two independent ways: IR temperature field and more precise thermocouple data in several points

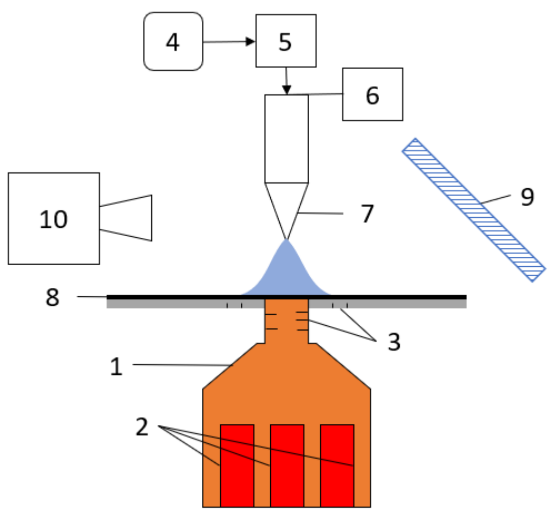

Figure 1: The scheme of experimental setup. 1 - Copper heater body, 2 - Cartridge heaters, 3 - Thermocouple, 4 - Compressor, 5 - Gas flow regulator (flowmeter), 6 - Pressure sensor, 7 - Nozzle, 8 - Black paint, 9 - IR Mirror, 10 - IR camera.

During the experiment, the gas flow rate and the power supplied to the heater were varied. For each given power and gas flow rate, it was necessary to wait a long time (about an hour) until thermal equilibrium was established. Based on the measured temperatures, the generated heat flux and heater surface temperature were determined. In the experiment, the heat transfer coefficient was determined using the following formula:

$$\alpha = \frac{q}{T_w - T_{in}} \tag{3}$$

where q is removed heat flux, T_w is temperature of the heater nozzle calculated or measured by IR camera, T_{in} is inlet air temperature.

To validate numerical simulation, which gives temperature distribution, we covered the top of the copper heater and stainless steel plate with a special black paint. This coating provides high emissivity in infrared part of the spectrum (Fig. 1(8), Fig. 2).

Since imaging from above is impossible, we attached IR mirror with 45° incline (Fig. 1(9)) and captured the surface temperature with IR camera Titanium 570M (Fig. 1(10)). The resulting apparent emissivity of the surface was equal to 0.88.

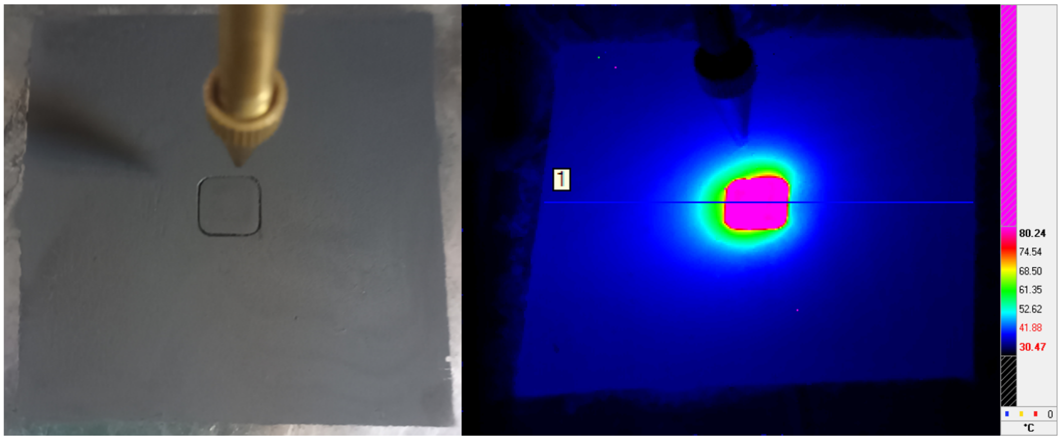

Figure 2: Photo (left) and infrared image of experimental setup (right). Line 1 shows cross-section for temperature field comparison.

3 Numerical simulation

ANSYS FLUENT 2020 R2 software is used to solve the conjugate heat transfer stationary problem in copper heater and steel plate subjected to an impact of turbulent air jet. The software, operating on a finite volume methodology, allows one to solve transient and steady-state problems, providing parallel computation functionalities. The shear-stress transport (SST) k-ω turbulence model introduced by Menter [34] was used. The model combines the formulation of the k-w in the near-wall region and the k-ϵ model in the flow region. The relevant blending functions are used to convert the k-ϵ model into a k-ω formulation. The governing equations of the flow field including continuity equation, momentum equations, and transport equations of k and w can be written as follows:

$$\frac{\partial u_i}{\partial x_i} = 0, \tag{4}$$

$$u_j \frac{\partial}{\partial x_j} u_i = -\frac{1}{\rho}\frac{\partial p}{\partial x_i} + \frac{\partial}{\partial x_j}(\nu + \nu_t)\frac{\partial}{\partial x_j} u_i, \tag{5}$$

$$\frac{\partial}{\partial x_j} k u_j = \frac{\partial}{\partial x_j}(\nu + \frac{\nu_t}{\sigma_k})\frac{\partial}{\partial x_j} k + \widetilde{G_k} - \beta^* k w, \tag{6}$$

$$\frac{\partial}{\partial x_j} w u_j = \frac{\partial}{\partial x_j}(\nu + \frac{\nu_t}{\sigma_w})\frac{\partial}{\partial x_j} w + G_w - \beta_i w^2 + 2(1 - F_1)\sigma_{w,2}\frac{1}{w}\frac{\partial k}{\partial x_j}\frac{\partial w}{\partial x_j}, \tag{7}$$

where u_j - gas velocity, p - hydrodynamic pressure, ν - kinematic viscosity of air, ν - turbulent viscosity, ρ - air density, k - turbulence kinetic energy, w - specific dissipation rate, σ_k and σ_w - turbulent Prandtl numbers for k and ω equal to:

$$\sigma_k = \frac{1}{\frac{F_1}{\sigma_{k,1}} + \frac{1-F_1}{\sigma_{k,2}}}, \tag{8}$$

$$\sigma_w = \frac{1}{\frac{F_1}{\sigma_{w,1}} + \frac{1-F_1}{\sigma_{w,2}}}, \tag{9}$$

the model constants $\sigma_{k,1}$, $\sigma_{k,2}$ and $\sigma_{w,1}$,$\sigma_{w,2}$ are 1.176, 1.0, 2.0, 1.168 respectively. The turbulent viscosity ν_t is determined as follows:

$$\nu_t = \frac{k}{\omega}\frac{1}{max[\frac{1}{\alpha*}, \frac{SF_2}{\alpha_1\omega}]} \tag{10}$$

$\alpha_1 = 0.31$. The coefficient α^* damps the turbulent viscosity causing a low-Reynolds-number correction. It is given by

$$\alpha^* = \alpha^*_\infty \frac{0.024 + Re_t/6}{1 + Re_t/6} \tag{11}$$

$Re_t = \nu k/\omega$ is the turbulent Reynolds number, $\alpha^*_\infty = 1$. The blending functions F_1 and F_2 are given by

$$F_1 = tanh([min[max(\frac{\sqrt{k}}{0.09wy}, \frac{500\nu}{wy^2}), \frac{4\rho k}{\sigma_{w2}D^+_w y^2}]]^4), \tag{12}$$

$$D^+_w = max[\frac{2\rho}{\sigma_{w2}}\frac{\partial k}{\partial x_j}\frac{\partial w}{\partial x_j}, 10^{-10}], \tag{13}$$

$$F_2 = tanh([max(\frac{\sqrt{k}}{0.09wy}, \frac{\nu}{y^2 w}]^2), \tag{14}$$

where y is the distance to the next surface. The production of turbulence kinetic energy $\widetilde{G_k}$ is defined as:

$$\widetilde{G_k} = min(G_k, 10\beta^* kw), \tag{15}$$

$$G_k = \nu_t S^2, \tag{16}$$

Where $S = \sqrt{2S_{ij}S_{ij}}$, $S_{ij} = \frac{1}{2}(\frac{\partial u_i}{\partial x_j} + \frac{\partial u_j}{\partial x_i})$. The production of ω is

$$G_w = \widetilde{G_k}\frac{\alpha_\infty}{\nu_t}, \tag{17}$$

α_∞ is defined as follows:

$$\alpha_\infty = F_1\alpha_{\infty,1} + (1 - F_1)\alpha_{\infty,2}, \tag{18}$$

$$\alpha_{\infty,1} = \frac{\beta_{i,1}}{\beta^*_\infty} - \frac{\kappa^2}{\sigma_{w,1}\sqrt{\beta^*_\infty}}, \tag{19}$$

$$\alpha_{\infty,2} = \frac{\beta_{i,2}}{\beta^*_\infty} - \frac{\kappa^2}{\sigma_{w,2}\sqrt{\beta^*_\infty}}, \tag{20}$$

where the model constants $\kappa = 0.41$, $\beta_{i,1} = 0.075$, $\beta_{i,2} = 0.0828$, β^*_∞=β^*= 0.09. The term included in the dissipation of w in equation (7) β_i equal to:

$$\beta_i = F_1\beta_{i,1} + (1 - F_1)\beta_{i,2}, \tag{21}$$

The energy equation is defined as:

$$u_j\frac{\partial}{\partial x_j}T = \frac{1}{\rho C_p}\frac{\partial}{\partial x_j}((\lambda + \lambda_t)\frac{\partial}{\partial x_j}T, \tag{22}$$

the equation (22) is resolved for gas phase, T - gas temperature, C_p - specific heat capacity of gas, λ - heat transfer coefficient of gas, $\lambda_t = C_p\mu/Pr_t$ - turbulent heat transfer coefficient, $Pr_t = 0.85$ - turbulent Prandtl number. For solid domains, the Laplace equation for temperature is solved with appropriate boundary conditions. Heat flux density conservation conditions is used for conjugate heat transfer. Thermal resistance is not considered in the model. The properties of air, steel and copper are summarized in Table 1.

domains	ρ, Kg/m^3	λ, W/mK	C_p, J/KgK	$\mu, kg/ms$
air	1.225	0.0242	1006.43	1.7894 10^{-5}
copper	8978	387.6	381	–
steel	8030	16.27	502.48	–

Table 1: Density, thermal conductivity, specific heat capacity and dynamic viscosity for air, copper and steel.

The velocity and pressure fields were linked by Coupled algorithm. The pressure staggering option was used to solve the continuity equation. The least squares cell-based algorithm was used to obtain the gradients. The convective terms for momentum and energy equations were discretized using the second-order upwind scheme. First-order upwind scheme was used for turbulent kinetic energy and specific dissipation rate equations.

The schematic diagram of computational domain with boundary conditions is shown in the fig.3. The problem was solved in a three-dimensional formulation. 1/4 of the region with the corresponding symmetry conditions was resolved (as shown in the fig.3). A fixed temperature condition is placed on the bottom wall of the copper heater. This temperature is taken from the experimental data obtained by thermocouples. An adiabatic boundary condition is placed on the bottom wall of the steel plate. A fixed temperature condition, taken from thermal camera data, was placed on the lateral outer walls of the steel plate. Pressure outlet conditions were placed on the outer walls of the air domain. The backflow turbulent intensity I was 10^{-3}. The turbulence intensity I is defined as the ratio of the root-mean-square of the velocity fluctuations u' to the mean flow velocity. Backflow turbulent viscosity ratio defined on that regions was $\mu_t/\mu = 10$ and backflow temperature was 296.16 K.The velocity was set at the

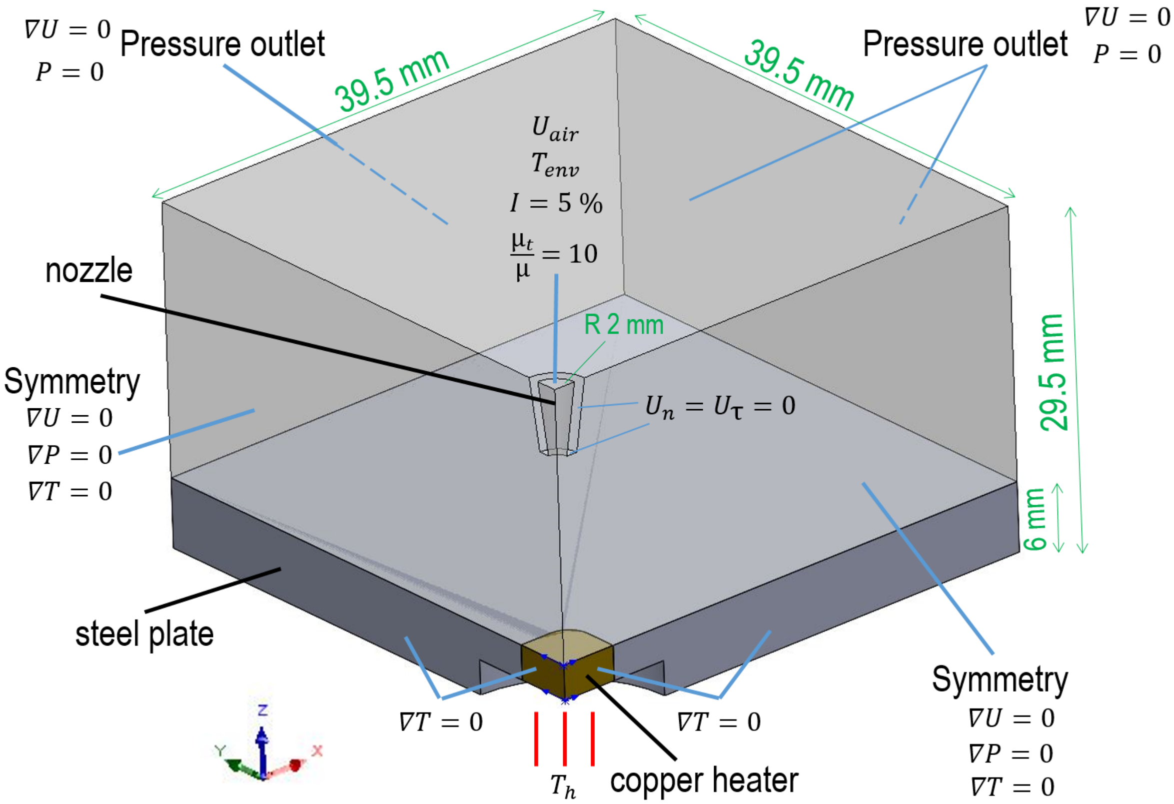

Figure 3: The schematic diagram of computational domain with boundary conditions.

nozzle inlet. The turbulent intensity and turbulent viscosity ratio are 5 10^{-2} and 10 respectively. The temperature T_{env} was 296.16 K.

An unstructured computational mesh was created to solve the problem (fig. 4). The number of tetrahedral elements was 4825262, the number of nodes was 1064865. The size of the elements a near the boundary between the air - steel domain was approximately 100 μm. $a = 100$ μm near the boundary between the air - copper. The element size after the nozzle was also approximately 100 μm. A grid independence study was conducted at the largest Reynolds number $Re = 10533$. The heat flux q was 186 kW/m^2. Three grids with different element sizes were considered: a) Coarse - the element size near the boundary between steel-air and copper-air was 1000 μm. The element size after the nozzle was also 1000 μm. b) Middle - the element size near the boundary between steel-air and copper-air was 500 μm. The element size after the nozzle was 500 μm. c) Fine - the element size near the boundary between steel-air and copper-air was 100 μm. The element size after the nozzle was 100 μm. Fig.5 a) shows the temperature distribution on the upper part of the metal plate in contact with air jet. The temperature distribution is almost independent on the mesh size. Also, the local Nusselt number $Nu = \alpha L_0/\lambda_{air}$ was used as another parameter to investigate the grid independence, where α - heat transfer coefficient, L_0 - characteristic length equal to the distance from the nozzle to the heater, λ_{air} - air thermal conductivity. Fig.5 b) shows the local Nusselt number on the upper part of the metal plate in contact with turbulent air jet. It turned out that Nu is sensitive to the size of grid elements, but

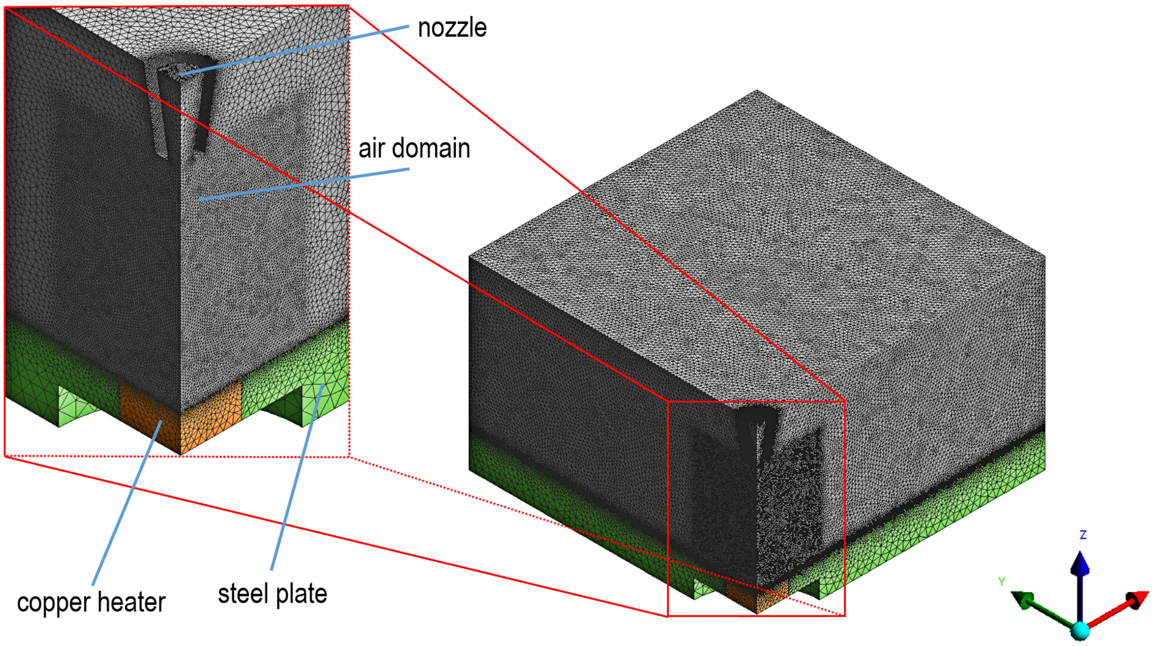

Figure 4: Computational grid.

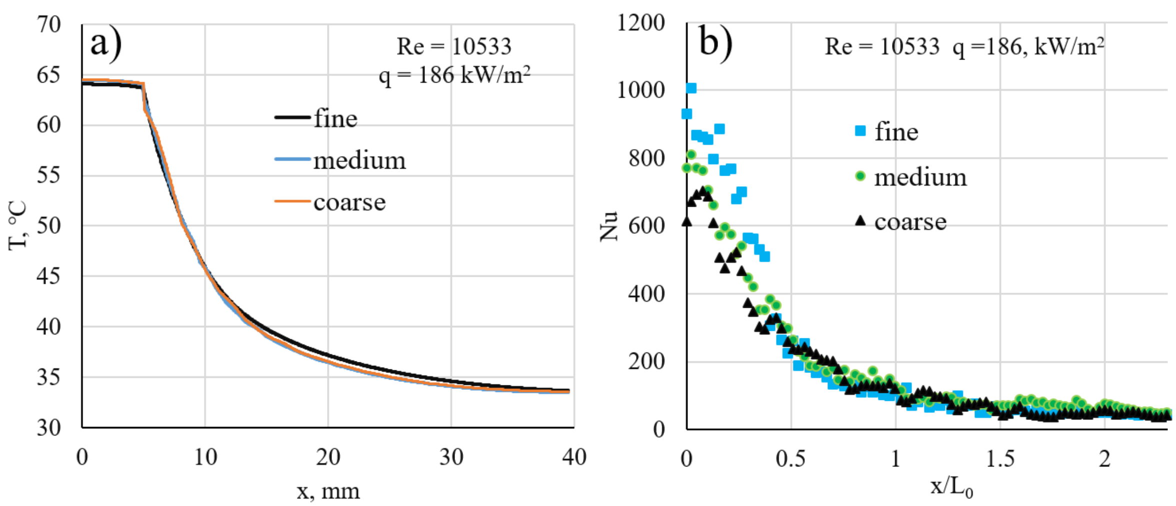

Figure 5: Grid independence test. a) Temperature dependence on the coordinate x, b) local Nusselt number Nu dependence on the dimensionless coordinate x/L_0, $L_0 = 17$ mm - the distance from nozzle to copper heater.

the difference in the integral Nusselt values is insignificant.

4 Results and discussion

The numerical simulation data of velocity field and streamlines for impact of turbulent air jet for different Reynolds numbers are shown in the fig.6. The Reynolds number was calculated using the formula $\mathrm{Re} = UD/\nu$, U denotes the average flow rate and

$D = 1$ mm represents the nozzle diameter. Fig. 6 d) shows that the air velocity is quite high in the heating region and almost damped in the steel plate region.

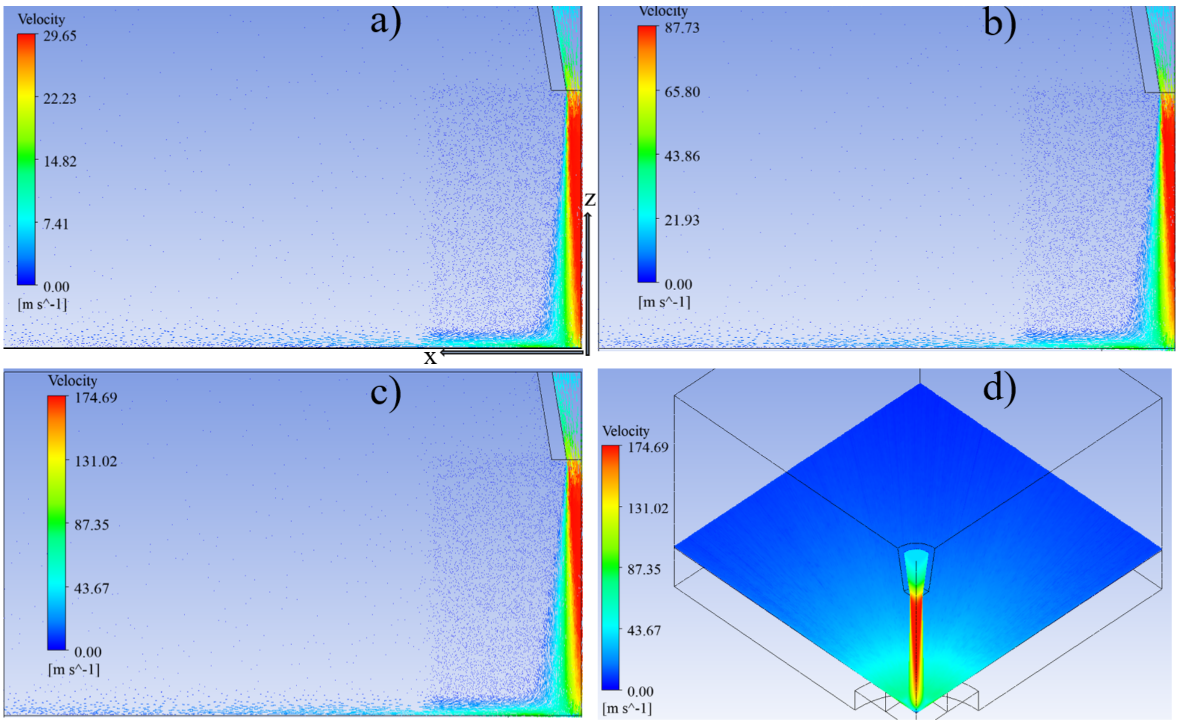

Figure 6: Velocity vector fields a) $Re = 1756$, b) $Re = 5266$, c) $Re = 10533$ as well as streamlines d) $Re = 10533$.

Comparative analysis of the temperature profiles obtained by the numerical simulations and the infrared camera data are presented in fig. 7 a,b,c. The comparison was made for different Reynolds numbers and for different heat fluxes. The prediction of the numerical simulations in the heater region are in good agreement with experimental observations. However there is a discrepancy in the steel plate region. The main reason is that the contact thermal resistance between copper and steel was not taken into account in the modeling. Experimental data show a temperature jump at the transition from the copper heater region to the steel plate due to contact thermal resistance. It should be noted that the discrepancy between the simulation and experimental data decreases as the velocity of the flow impinging on the plate increases. This is due to the increase in the heat transfer coefficient on the copper heater with increasing flow velocity, which is demonstrated in fig.7 d. Fig. 7 d shows the distribution of the local Nusselt number with respect to the dimensionless coordinate x$/L_0$, where L_0 is the distance from the nozzle to the heater. The local Nusselt number increases in the stagnation region with increasing velocity of the impinging turbulent flow and practically does not change in the region of the steel plate.

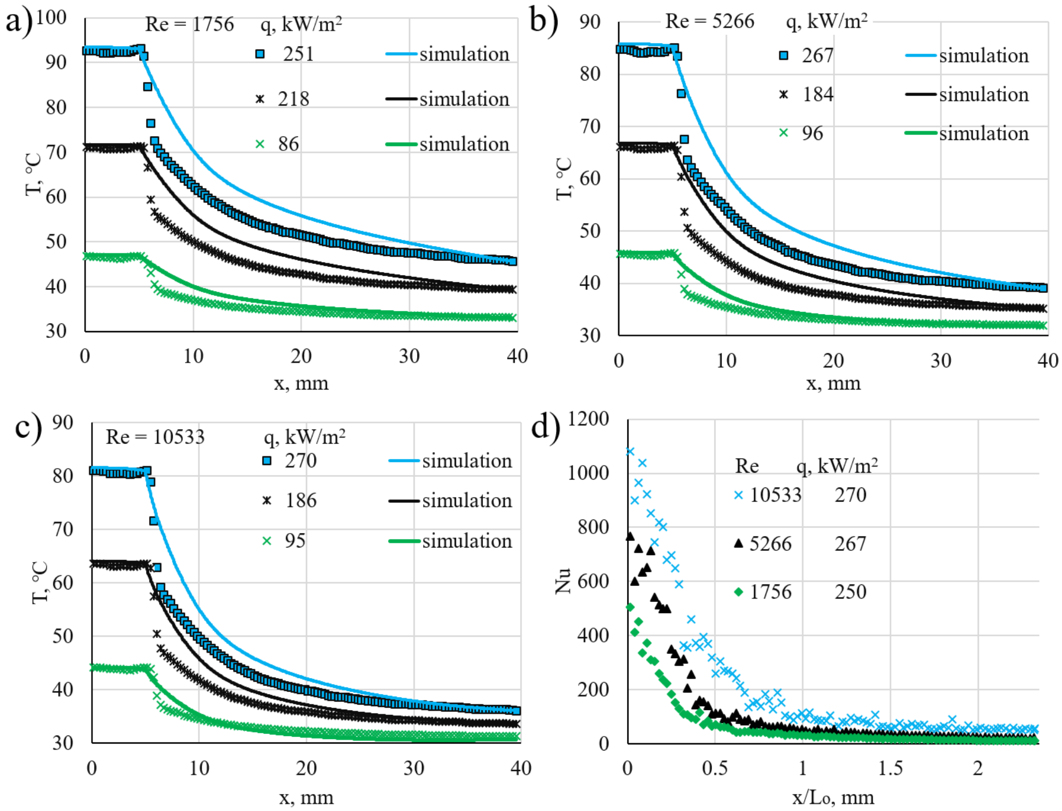

Figure 7: Comparison of the temperature profile obtained by the infrared camera with numerical simulation data a)$Re = 1756$, b) $Re = 5266$, c)$Re = 10533$ and local Nusselt number for different Reynolds numbers d) obtained by numerical simulation.

Conclusion

An investigation was conducted to examine steady-state conjugate heat transfer in a turbulent air jet impinging on a stainless steel plate with a copper rod acting as a heater at its center. The study involved experimental and numerical analyses in three-dimensional formulation by the finite volume method. The turbulence shear-stress transport (SST) $k - \omega$ model was utilized in the numerical simulation. Comparisons between temperature profiles obtained through infrared scanning and numerical simulations revealed good agreement within the copper heater region. Discrepancies observed in the steel plate region were attributed to contact thermal resistance between the steel and copper materials. The local Nusselt number exhibited an increase in the stagnation region with higher impinging flow velocities, while remaining relatively constant in the steel plate region.

Acknowledgement

Research reported in this paper was financially supported by the Russian Science Foundation (Project No. 21-79-10373, https://rscf.ru/project/21-79-10373/).The IR-camera was carried out under the state contract with IT SB RAS.

References

[1] Zaitsev D.V., Belosludtsev V.V., Tkachenko E.M., Ye F., Guo H., Cheverda V.V., Kabov O.A., *Shear-driven liquid films in a channel under intense local heating: methodology and critical heat flux results*, Interfacial Phenom. Heat Transf., 10. 2 (2022), 53-65.

[2] Cheverda V.V., Kabov O.A., *An experimental study of rivulet flow in low-boiling liquid driven by gas flow in a minichannel*, Tech. Phys. Lett., 43. 3 (2017), 293-296.

[3] Kabov O.A., Zaitsev D.V., Cheverda V.V., Bar-Cohen A., *Evaporation and flow dynamics of thin, shear-driven liquid films in microgap channels*, Exp. Therm. Fluid. Sci., 35. 5 (2011), 821-831.

[4] Dementyev Y.A., Chinnov E.A., Kochkin D.Y., Ronshin F.V, Evstrapov A.A, Gusev V.S, Kabov O.A., *An experimental investigation of adiabatic two-phase flow patterns in a slit microchannel with 1:800 aspect ratio*, Exp. Therm. Fluid. Sci., 154 (2024), 111153.

[5] Sibiryakov N., Dimov S., Kabov O.A., *Measurement of the heat transfer coefficient in gas spray cooling with low liquid flow rate*, E3S Web of Conferences.- EDP Sciences, 459 (2023), 04013.

[6] Spalding D.B., *A unified theory of friction, heat transfer and mass transfer in the turbulent boundary layer and wall jet.*, ARC Rep., London, (1965) 25925.

[7] Gauntner J.W., *Survey of literature on flow characteristics of a single turbulent jet impinging on a flat plate.*, NASA (1970).

[8] Jambunathan K. et al., *A review of heat transfer data for single circular jet impingement.*, Int. J. Heat Fluid Flow, 13. 2 (1992), 106-115.

[9] Carlomagno G.M., Ianiro A., *Thermo-fluid-dynamics of submerged jets impinging at short nozzle-to-plate distance: A review.*, Exp. Therm. Fluid Sci., 58 (2014), 15-35.

[10] Launder B.E., Rodi W., *The turbulent wall jet measurements and modeling.*, Annu. Rev. Fluid Mech., 15. 1 (1983), 429-459.

[11] Ekkad S.V., Singh P.A., *A modern review on jet impingement heat transfer methods.*, J. Heat Transf., 143. 6 (2021), 064001.

[12] Barewar S.D. et al., *Optimization of jet impingement heat transfer: A review on advanced techniques and parameters.*, TSEP, 39 (2023), 101697.

[13] Zuckerman N., Lior N., *Jet Impingement Heat Transfer: Physics, Correlations, and Numerical Modeling.*, Adv. Heat Transf., 39 (2006), 565-631.

[14] Dairay T. et al., *Direct numerical simulation of a turbulent jet impinging on a heated wall*, J. Fluid Mech., 764 (2015), 362-394.

[15] Attalla M., Salem M., *Experimental investigation of heat transfer for a jet impinging obliquely on a flat surface*, Exp. Heat Transf., 28. 4 (2015), 378-391.

[16] Abhishek M. et al., *Experimental study of flow characteristics of an oblique impinging jet*, Exp. Fluids., 61. 3 (2020), 1-16.

[17] Modak M. et al., *Theoretical and experimental study on heat transfer characteristics of normally impinging two dimensional jets on a hot surface*, Int. J. Therm. Sci., 112 (2017), 174-187.

[18] Hout R., Rinsky V., Grobman Y., *Experimental study of a round jet impinging on a flat surface: flow field and vortex characteristics in the wall jet*, Int. J. Heat Fluid Flow, 70 (2018), 41-58.

[19] Shariatmadar H. et al., *Experimental and numerical study on heat transfer characteristics of various geometrical arrangement of impinging jet arrays*, Int. J. Therm. Sci., 102, (2016), 26-38.

[20] Tang Z. et al., *Numerical simulation of heat transfer characteristics of jet impingement with a novel single cone heat sink*, Appl. Therm. Eng., 127 (2017), 906-914.

[21] Rakhsha S., Zargarabadi R., Saedodin S., *Experimental and numerical study of flow and heat transfer from a pulsed jet impinging on a pinned surface*, Exp. Heat Transf., 34. 4 (2021), 1-16.

[22] Ortega-Casanova J., Granados-Ortiz F., *Numerical simulation of the heat transfer from a heated plate with surface variations to an impinging jet*, Int. J. Heat Mass Transf., 76 (2014), 128-143.

[23] Wen Z. et al., *Numerical study of impinging jets heat transfer with different nozzle geometries and arrangements for a ground fast cooling simulation device*, Int. J. Heat Mass Transf., 95 (2016), 321-335.

[24] Behnia M. et al., *Numerical study of turbulent heat transfer in confined and unconfined impinging jets*, Int. J. Heat Mass Transf., 20 (1999), 1-9.

[25] Huang L. et al., *An experimental and numerical study on heat transfer enhancement of a heat sink fin by synthetic jet impingement*, Heat Mass Transf., 57 (2021), 583-593.

[26] Dutta P., Chattopadhyay H., *Numerical analysis of transport phenomena under turbulent annular impinging jet*, Comput.Therm. Sci.: Int. J., 13. 2 (2021), 1-19.

[27] Yang Y.T., Tsai S.Y., *Numerical study of transient conjugate heat transfer of a turbulent impinging jet*, Int. J. Heat Mass Transf., 50 (2007), 799-807.

[28] Poh H., Kumar K., Mujumdar A., *Heat transfer from a pulsed laminar impinging jet*, Int. Commun. Heat Mass Transf., 32 (2005), 41-58.

[29] Peng X. et al., *Heat transfer under a pulsed slot turbulent impinging jet at large temperature differences*, Therm. Sci., 14.1 (2010), 271-281.

[30] Bejera R., Duttaand P., Srinivasan K., *Numerical study of interrupted impinging jets for cooling of electronics*, IEEE Trans. Compon. Packag. Technol., 30. 2 (2007), 275-284.

[31] Esmailpour K. et al., *A numerical study of heat transfer in a turbulent pulsating impinging jet.*, Appl. J. Chem. Eng., 93 (2015), 959-969.

[32] Lemanov V.V., Pakhomov M.A., Terekhov V.I., *Experimental and numerical simulation of heat transfer in an impact synthetic jet*, High Temp., 61, (2023), 206-212.

[33] Li P., Huang X., Guo D., *Numerical analysis of dominant parameters in synthetic impinging jet heat transfer process*, Int. J. Heat Mass Transf., 150, (2020), 119280.

[34] Menter F.R., *Two-Equation Eddy-Viscosity Turbulence Models for Engineering Applications.*, AIAA J., 32. 8 (1994), 1598-1605.

Mungalov A. S.,
Kutateladze Institute of Thermophysics of Siberian Branch of Russian Academy of Sciences,
1, Lavrentiev avenue, 630090, Novosibirsk, Russia,
Email: a.mungalov@alumni.nsu.ru,

Sibiryakov N. E.,
Kutateladze Institute of Thermophysics of Siberian Branch of Russian Academy of Sciences,
1, Lavrentiev avenue, 630090, Novosibirsk, Russia,

Kochkin D. Y.,
Kutateladze Institute of Thermophysics of Siberian Branch of Russian Academy of Sciences,
1, Lavrentiev avenue, 630090, Novosibirsk, Russia,

Cheverda V. V.,
Kutateladze Institute of Thermophysics of Siberian Branch of Russian Academy of Sciences,
1, Lavrentiev avenue, 630090, Novosibirsk, Russia,

Somvanshi P. M.,
Kutateladze Institute of Thermophysics of Siberian Branch of Russian Academy of Sciences,
1, Lavrentiev avenue, 630090, Novosibirsk, Russia,
Department of Mechanical Engineering, Indian Institute of Technology Kanpur, Kanpur 208016, India,

Kabov O. A.,
Kutateladze Institute of Thermophysics of Siberian Branch of Russian Academy of Sciences,
1, Lavrentiev avenue, 630090, Novosibirsk, Russia,

Received 08.05.2024, Accepted 25.06.2024